



Article

Design of Dyes Based on the Quinoline or Quinoxaline Skeleton towards Visible Light Photoinitiators

Ilona Pyszka * and Beata Jędrzejewska

Faculty of Chemical Technology and Engineering, Bydgoszcz University of Science and Technology,
Ul. Seminaryjna 3, 85-326 Bydgoszcz, Poland; beata@pbs.edu.pl
* Correspondence: ilona.pyszka@pbs.edu.pl; Tel.: +48-52-374-9039

Abstract: Dyes based on quinoline and quinoxaline skeletons were designed for application as visible light photoinitiators. The obtained compounds absorb electromagnetic radiation on the border between ultraviolet and visible light, which allows the use of dental lamps as light sources during the initiation of the photopolymerization reaction. Their another desirable feature is the ability to create a long-lived excited state, which enables the chain reaction to proceed through the mechanism of intermolecular electron transfer. In two-component photoinitiating systems, in the presence of an electron donor or a hydrogen atom donor, the synthesized compounds show excellent abilities to photoinitiate the polymerization of acrylates. In control tests, the efficiency of photopolymerization using modified quinoline and quinoxaline derivatives is comparable to that obtained using a typical, commercial photoinitiator for dentistry, camphorquinone. Moreover, the use of the tested compounds requires a small amount of photoinitiator (only 0.04% by weight) to initiate the reaction. The research also showed a significant acceleration of the photopolymerization process and shortening of the reaction time. In practice, this means that the new two-component initiating systems can be used in much lower concentrations without slowing down the speed of obtaining polymer materials. It is worth emphasizing that these two features of the new initiating system allow for cost reduction by reducing financial outlays on both materials (photoinitiators) and electricity.

Keywords: photopolymerization; UV-Vis initiators; quinoline derivatives; quinoxaline derivatives; two-component initiating systems



Citation: Pyszka, I.; Jędrzejewska, B. Design of Dyes Based on the Quinoline or Quinoxaline Skeleton towards Visible Light Photoinitiators. *Int. J. Mol. Sci.* **2024**, *25*, 4289. <https://doi.org/10.3390/ijms25084289>

Academic Editor: Raphaël Schneider

Received: 20 March 2024

Revised: 9 April 2024

Accepted: 10 April 2024

Published: 12 April 2024



Copyright: © 2024 by the authors. Licensee MDPI, Basel, Switzerland. This article is an open access article distributed under the terms and conditions of the Creative Commons Attribution (CC BY) license (<https://creativecommons.org/licenses/by/4.0/>).

1. Introduction

A huge problem in the modern world is global climate change, caused mainly by carbon dioxide emissions. It is related to the processes of burning fossil fuels in electricity generation and heat production, transportation and industry. The energy sector is the source of about three-quarters of global greenhouse gas emissions [1]. Switching to renewable energy sources such as solar, wind and hydropower and improving energy efficiency are essential to save the environment. Nowadays, increased attention is paid to the amount of energy used in chemical reactions. Therefore, it is increasingly proposed to apply light as an energy source [2]. Most photochemical-based manufacturing processes can effectively avoid high energy consumption, which is crucial in practical industrial production.

In recent years, the most innovative technologies for producing polymeric materials are based on processes initiated photochemically, i.e., with light [3–8]. This technique is quite common nowadays. The range of applications of photopolymerization is also confirmed by the growing interest in photoinitiating systems operating in the visible light range. It is worth noting that the most popular applications of photopolymerization include dentistry, 3D/4D printing and coating [9–19]. Moreover, the synthesis of polymeric materials conducted by photopolymerization is one of the most efficient methods. Due to the low energy consumption, lack of solvents and the high speed of the process at ambient temperature, photopolymerization is also an environmentally friendly technique [10]. The

growing interest in photopolymerization processes leads to research aimed at increasing the efficiency of the process of obtaining polymers using visible light. This is mainly because visible light, compared to ultraviolet light, is cheaper, safer and has a greater ability to penetrate deep into the polymerizing mixture [20].

However, commercial initiators used in industry—compounds responsible for starting photopolymerization processes—have significant limitations. The photoinitiators used so far absorb visible light to a small extent. This is an extremely important technological problem for their versatile applications because these compounds absorb radiation emitted by cheap light sources in an ineffective way.

Photoinitiators, next to co-initiators, monomers and additives responsible for the specific functional requirements of the materials, are the main components of photopolymerization systems. The photoinitiator plays a key role in the photoinitiation system and therefore in the entire photopolymerization process, because it directly determines the photopolymerization rate and also affects the physical and mechanical properties of the polymerized materials [21]. According to the type of photoinitiator used, the photopolymerization reaction can be divided into free radical photopolymerization, cationic photopolymerization and anionic photopolymerization [22]. In the case of the former, photoinitiators must have the ability to absorb light in the appropriate spectral range (UV or Vis) [23,24]. When exposed to UV or visible light, photoinitiators absorb photons and then undergo subsequent reactions out of the excited state, creating free radicals capable of inducing a chain reaction. When multifunctional monomers are used, cross-linked structures are created [25].

Photoinitiators of free radical polymerization, depending on the mechanism of radical formation, are divided into two main groups, i.e., type I and type II [26–28]. Type I photoinitiators are directly cleaved upon irradiation to generate initiating radicals, while type II photoinitiators generate radicals by photoinduced electron transfer (PET) between the photoinitiator and co-initiator [29–32]. Type II photoinitiators are aromatic ketones, e.g., benzophenone [33], as well as cyanines [34], phenazines [35] and many others [32,36–40]. Among them, there are those that have good light absorption properties and high initiation efficiency in the UV region, which makes them extremely popular photoinitiators in the field of UV curing.

The co-initiators are usually electron donors, i.e., aromatic amines or sulfur compounds [24,41,42]. However, amine additives are often toxic [43]. Due to this serious drawback, new co-initiators with low toxicity are being sought.

Owing to certain inconveniences associated with the use of commercial photoinitiators, there was a need to develop new, universal and effective photoinitiator systems that would be more sensitive to visible light sources. Therefore, an attempt was made to obtain effective photoinitiators by modifying the structure of dyes containing quinoline and quinoxaline skeletons to improve the photoinitiating properties in the visible region. The aim of the research was also to significantly accelerate the process, shorten the polymerization time and reduce the concentration of the initiating system and, thus, reduce costs resulting from lower financial outlays on both materials (photoinitiators) and electricity. In practice, this means that new two-component initiating systems can be used in much lower concentrations without slowing down the speed of obtaining polymer materials. The commercial attractiveness of the designed initiating systems results from the possibility of their use in the dental industry for obtaining light-cured dental fillings, in medicine for obtaining hydrogel polymeric materials, as well as in modern imaging techniques using 3D printing.

2. Results and Discussion

2.1. Designing the Structure of the Dyes

Five compounds containing a quinoline (DQ1, DQ2) or quinoxaline (DQ3, DQ4, DQ5) skeleton were synthesized. The selection of compounds containing a nitrogen-based heterocyclic ring allows with high probability to design compounds with biological, chemotherapeutic and pharmacological applications, such as antirheumatic and antihis-

tamine drugs [44,45]. Moreover, 2-aminopyridine, quinoline and quinoxaline have anticancer, antibacterial, antiviral, antimalarial and antifungal properties [46–50]. This is beneficial from the viewpoint of further potential use of these dyes as photoinitiators in dentistry. In addition, their structure was stiffened by condensation of several aromatic rings. This was intended to eliminate excited state deactivation channels by preventing the rotation of benzene rings and isomerization.

The criterion for selecting dyes was not only the ease of synthesis of these compounds, but also their spectroscopic properties. Therefore, the structure of the quinoline derivative DQ2 was modified to the quinoxaline derivative (DQ3, DQ4) to adjust the spectroscopic properties, especially the position and intensity of the absorption band, and to obtain compounds that effectively initiate polymerization upon visible light irradiation. The synthesized derivatives differ in the number of nitrogen atoms (DQ1–DQ5), the presence of a methyl substituent (DQ4), or an oxygen atom (DQ5).

The structure and purity of the dyes were confirmed by NMR spectroscopy. The lack of a signal at 3.0–5.0 ppm in the ^1H NMR spectra, indicating the presence of an amino group, confirmed the formation of a condensation product with a characteristic $-\text{C}=\text{N}-$ bond (signal at 150.0–160.0 ppm in the ^{13}C NMR spectrum). All synthesized compounds (DQ1–DQ5) were in the form of light-yellow crystals, and their solutions were pale yellow in color. This is especially important from the viewpoint of their potential use in dentistry because it allows for obtaining natural shades of fillings.

2.2. Spectroscopic Properties

The electronic absorption spectra of the synthesized dyes were recorded in ethyl acetate and are presented in Figure S1 in Supplementary Materials. On their basis, both the wavelength at which the absorption maximum occurs (λ_{max}) and the molar absorption coefficients (ϵ) were determined (Table 1).

Table 1. Spectroscopic and electrochemical properties, quantum yield of triplet state formation and triplet state lifetime of the tested dyes.

Dyes	^a $\lambda_{max}^{Abs.}$ (nm)	ϵ ($\text{M}^{-1} \text{cm}^{-1}$)	^b λ_{max}^{Fl} (nm)	Φ_{Fl}	λ_{max}^{Ph} (nm)	E_T^{00} (eV)	E_{red} (V)	^c ΔG_{el} (eV)
DQ1	387	2610	447	0.230	526	2.79	−1.054	−0.286
	408	3040	477		542			
	432	2360	511		572			
DQ2	316	14,400	406	0.176	510	2.51	−0.98	−0.08
	330	20,150						
	367	3980						
DQ3	334	14,100	465	0.039	543	2.74	−1.17	−0.12
	350	16,300			588			
	386	4200						
DQ4	334	14,100	476	0.040	515	2.95	−1.18	−0.32
	351	16,500			561			
	405	3400						
DQ5	287	34,600	443	0.123	529	2.72	−1.09	−0.18
	381	3500						
CQ	472	40	-	-	-	-	-	-

^a measured in ethyl acetate, ^b measured in 2-methyltetrahydrofuran, ^c ΔG_{el} calculated for PhTAA ($E_{ox} = 1.450$ V) as co-initiator.

Unsubstituted quinoline (QL) and quinoxaline (QX) absorb electromagnetic radiation in the UV region. The absorption maxima of these compounds are at 204, 225 and 276 nm for QL [45] and at 314 nm for QX [51]. The data collected in Table 1 and shown in Figure S1 indicate that the modification of these structures clearly affects the position of the absorption bands and induces the bathochromic effect. DQ2 and DQ3 dyes absorb electromagnetic radiation on the border between ultraviolet and visible light region. How-

ever, the absorption maxima of DQ1 and DQ4 dyes are in the visible range, or, as in the case of DQ5, the absorption bands are wide and overlap the visible region. Thanks to this, they can absorb light emitted by the dental lamp used in the photopolymerization process. Moreover, their molar absorption coefficients at 400 nm range from $3000 \text{ M}^{-1} \text{ cm}^{-1}$ to $4000 \text{ M}^{-1} \text{ cm}^{-1}$ and are approximately 500 times higher than those of camphorquinone ($8 \text{ M}^{-1} \text{ cm}^{-1}$ at 400 nm), a standard photoinitiator used in dentistry.

Furthermore, the modification of the quinoline skeleton (DQ2) to 2-oxo-2,3-dihydro-1*H*-imidazo[1,2-*a*]pyridinium bromide (DQ1) (Figure S1) causes a change in the shape of the absorption band and shifts its maximum to a long wavelength by approximately 70 nm (bathochromic effect). The DQ1 dye has an electronic absorption spectrum characterized by several maxima in the long-wavelength part of the spectrum. This is typical for heterocyclic aromatic compounds with fused rings. However, the modification of the quinoline ring (DQ2) to quinoxaline (DQ3 and DQ4) does not change the shape of the absorption bands but only shifts them towards longer wavelengths by 18–38 nm (Figure S1). The electronic absorption spectra of these dyes are characterized by an intense absorption band located in the range of 320–350 nm and a second, less intense absorption band shifted by ca. 35–50 nm to the red. The presence of an oxygen atom in quinoxaline derivatives (DQ5) compared to the quinoline derivative (DQ2) causes a decrease in the intensity of the long-wavelength absorption band with a simultaneous bathochromic effect (Figure S1).

After absorbing electromagnetic radiation, the dye molecule returns to its ground state, emitting excess energy as electromagnetic radiation or heat. The emission spectra provide valuable information about the excited states of the molecule and the mechanism of energy transfer between them. The phenomenon of photoluminescence, both fluorescence and phosphorescence, was observed for the synthesized dyes.

Similarly to absorption spectra, the wavelength at which the fluorescence and phosphorescence maximum occurs depends on the structure of the synthesized dyes. The data presented in Figure S2a,b indicate the bathochromic effect observed because of the modification of the structure of the DQ2 dye. Compound DQ1 has complex fluorescence with strong peaks occurring at 447, 477 and 511 nm. The remaining DQ2–DQ5 compounds have broad fluorescence bands with one maximum, shifting towards longer wavelengths with the increase in the number of nitrogen atoms in the molecule (DQ2 vs. DQ1, DQ3, DQ4) and the introduction of an oxygen atom (DQ2 vs. DQ5). This means that the introduction of additional nitrogen atoms in the dye molecule, and thus the modification of quinoline derivatives to quinoxaline, is responsible for shifting the fluorescence band to the longer wavelength (lower frequency).

In addition to fluorescence, the dyes tested also emit phosphorescence. The phosphorescence spectrum has a longer wavelength than the fluorescence spectrum because the energy of the triplet state is lower than the energy of the corresponding singlet state [49]. The spectra presented in Figure 1 illustrate the relationship between the absorption spectrum and emission spectra of the dye (DQ1) (the spectra for other dyes are included in Supplementary Materials—Figure S3) [52]. The energy values of the $T_1 \rightarrow S_0$ transition (E_T^{00}) were determined based on the phosphorescence spectra. The energy of the triplet state for the synthesized dyes ranges from 2.51 to 2.95 eV. The spectroscopic data are collected in Table 1.

Moreover, the fluorescence spectra of the synthesized dyes are a beautiful illustration of the principle of mirror image electronic absorption spectra (Figure 1).

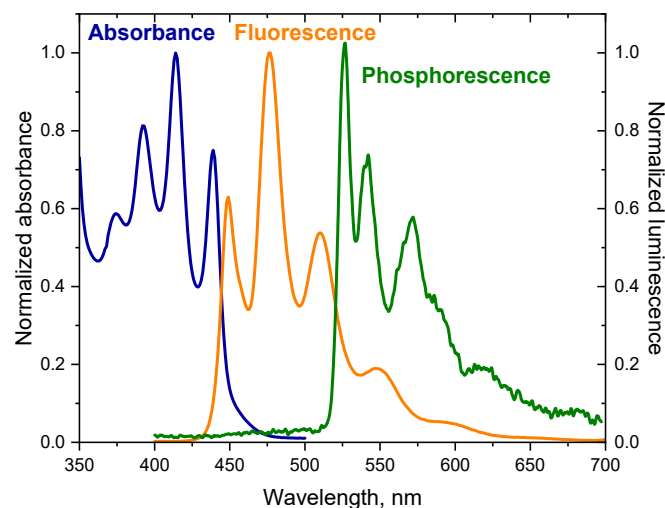


Figure 1. Electronic absorption spectrum, fluorescence and phosphorescence spectra of 2-oxo-2,3-dihydro-1*H*-imidazo[1,2-*a*]pyridinium bromide (DQ1) in 2-methyltetrahydrofuran. The phosphorescence spectrum was recorded at liquid nitrogen temperature; Ex = 350 nm.

The formation of the triplet state by the tested dyes was also confirmed by recording transient absorption spectra using the laser flash photolysis method. The spectral characteristics of the DQ1-DQ5 triplet state are shown in Figures 2 and S4 in the Supplementary Materials. After excitation of the dye with a laser light beam at 355 nm in a deoxygenated acetonitrile, both quinoline and quinoxaline derivatives show transient absorption that decays on a microsecond time scale. The absorption bands at 340–430 nm are attributed to triplet state absorption. The maxima of these bands depend on the dye structure, and are located at 390 nm, 430 nm, 370 nm, 360 nm and 340 nm for DQ1, DQ2, DQ3, DQ4 and DQ5, respectively. The analysis of the transient absorption kinetic curves (Figures 3 and S5 in Supplementary Materials) allowed to determine the lifetime of the triplet state. Its value is 1.52, 0.74, 1.31, 1.58 and 1.00 μs for DQ1, DQ2, DQ3, DQ4 and DQ5, respectively. It can be concluded that the lifetime of the triplet state of the DQ1 and DQ4 derivatives is approximately twice as long as that of the DQ2 derivative. The DQ1 and DQ4 derivatives also show higher intersystem transition efficiency compared to DQ2 and DQ3, as evidenced by the triplet state quantum yield values of 0.549, 0.006, 0.106, 0.632 and 0.270 for DQ1, DQ2, DQ3, DQ4 and DQ5, respectively (Table 2). The quantum yield of the triplet state was determined using the method described by Lament et al. [53] and by us [35].

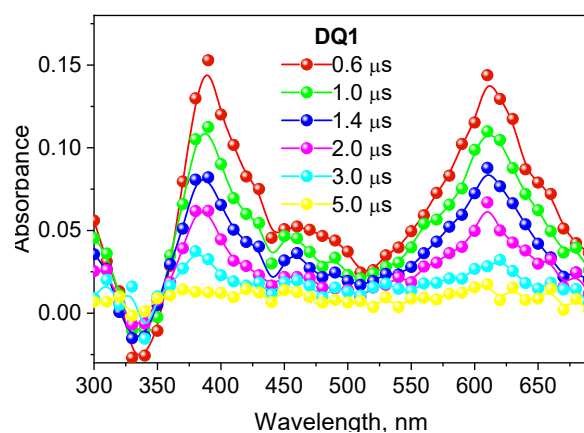


Figure 2. Absorption spectrum of the triplet state of 2-oxo-2,3-dihydro-1*H*-imidazo[1,2-*a*]pyridinium bromide (DQ1) recorded in deoxygenated acetonitrile.

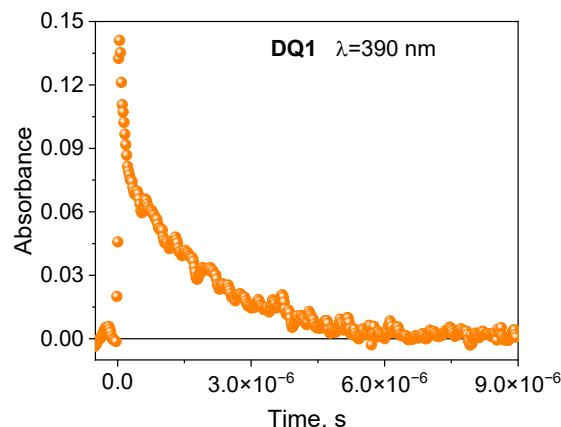


Figure 3. Kinetic curves of the disappearance of the triplet state recorded for 2-oxo-2,3-dihydro-1*H*-imidazo[1,2-*a*]pyridinium bromide (DQ1) at 390 nm.

Table 2. Quantum yield of triplet state formation (Φ_T) for the tested dyes and triplet state lifetime (τ_T).

Dyes	Φ_T	$\tau_T, \mu\text{s}$
DQ1	0.5490	1.52
DQ2	0.0060	0.74
DQ3	0.1061	1.00
DQ4	0.6320	1.58
DQ5	0.2704	1.31

The negative absorption with maximum at 390 nm, 430 nm, 370 nm, 360 nm and 340 nm for DQ1, DQ2, DQ3, DQ4 and DQ5, respectively, is due to photophysical processes and corresponds to the high ground-state absorption at these wavelengths (Figures 2 and S4).

The transient absorption spectra confirm that these compounds generate a triplet state. This is particularly important in the context of initiating the polymerization reaction. The triplet state of the synthesized dyes was effectively quenched by electron donors used in the tested photoinitiating systems: PhTAA, PhTACA, DMA, PhIAA, PhAA and PhPA. The quenching rate constants k_q (Table 3) were determined from the triplet–triplet transient absorption spectra at a specific wavelength, recorded at different quencher concentrations based on the classical Stern–Volmer equation [54] (Figure 4):

$$k_{obs} = \tau_T^{-1} + k_q[Q] \quad (1)$$

where: k_q —quenching rate constant of the excited state, τ_T —lifetime of the excited state in the absence of an electron donor, $[Q]$ —molar concentration of the quencher.

Table 3. Quenching constants of the triplet state of the tested dyes (k_q).

Co-Initiators	$k_q \times 10^{-8}, \text{M}^{-1} \text{s}^{-1}$				
	DQ1	DQ2	DQ3	DQ4	DQ5
PhTAA	25.10	9.66	13.40	24.71	18.00
PhTACA	5.20	3.01	3.12	6.25	5.30
DMA	6.94	3.16	3.98	7.09	5.92
PhIAA	16.20	6.62	8.92	17.80	12.30
PhAA	2.79	2.33	2.63	2.65	4.61
PhPA	3.02	2.75	2.98	3.12	5.05
MBX	3.36	1.97	2.01	2.98	3.11

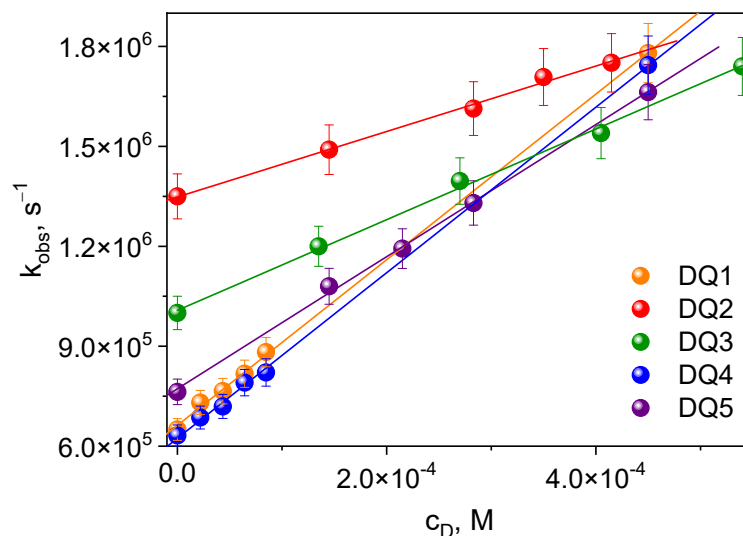


Figure 4. Stern–Volmer dependence of the triplet state quenching process for the tested dyes. Electron donor: thiophenoxyacetic acid.

If the only way to quench the triplet state is by the electron donor, it can be assumed that the quenching rate constant is equal to the electron transfer rate constant [27].

$$k_q = k_{el} \quad (2)$$

The research shows that the rate of quenching of the excited state depends on the structure of the dye. The triplet state of DQ1 and DQ4 dyes is effectively quenched by thiophenoxyacetic acid and other electron donors used; therefore, higher electron transfer rate constants are observed for them compared to the other dyes. Consequently, they should better initiate the polymerization of triacrylates.

2.3. Photopolymerization

Generally, free radicals that initiate photopolymerization are formed by the homolytic cleavage of bonds after the input of significant amounts of energy or by the electron transfer. In the latter, not only does light play a vital role, but so does the type of the second component in the photoinitiating composition since radicals are formed in bimolecular processes. During photoinduced intermolecular electron transfer (PET) processes [24,41,42], the excited electron is transferred from an electron donor (co-initiator) to an electron acceptor (dye). This process is effective if both molecules are at the right distance from each other. Therefore, in two-component photoinitiating systems without electrostatic interactions in the ground state, the diffusion and lifetime of the excited state of the molecule play a key role. After the electron transfer process, subsequent reactions occur, i.e., proton transfer, proton transfer and decarboxylation, as well as other reactions that lead to the formation of a radical that initiates polymerization. In addition to the PET mechanism, other classic photochemical reactions may occur to generate radicals that initiate the polymerization reaction, e.g., hydrogen atom transfer [41,55,56]. The dye molecule detaches a hydrogen atom from the co-initiator (MBX), creating two radicals. The resulting radicals can recombine with each other to give various products (Figure 5). The rate of the hydrogen atom transfer depends on the energy needed to break the bond between the hydrogen atom and the rest of the co-initiator molecule. The most commonly used hydrogen atom donors are amines, alcohols and thiols [57].

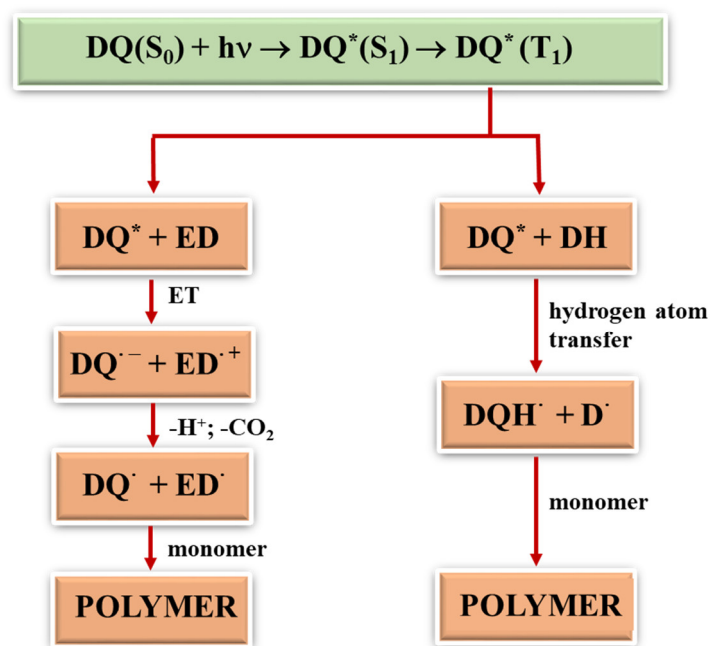


Figure 5. General mechanism of formation of radicals initiating polymerization; (*) the symbol denotes the excited state of the tested dyes (DQ).

As shown in Figures 1 and 2, the tested dyes form a long-lived triplet state, which makes them effective chromophores in two-component photoinitiating systems containing as co-initiator (electron donor or hydrogen donor) PhTAA, PhAA, PhPA, DMA, PhIAA, PhTACA and MBX. Due to the possibility of applying these compounds in dentistry, camphorquinone—a photoinitiator for dentistry—was used for comparative purposes.

2.3.1. Photoinitiation by the Mechanism of Intermolecular Electron Transfer Influence of the Photoinitiator Structure

Figure 6 shows exemplary kinetic curves recorded during photoinitiation of free radical polymerization of TMPTA initiated by synthesized dyes in the presence of the electron donor, PhTAA. The analysis of the kinetic curves and the initial rates of photoinitiated polymerization collected in Table 4 prove that the efficiency of TMPTA photoinitiation depends on the structure of the quinoline and quinoxaline derivatives.

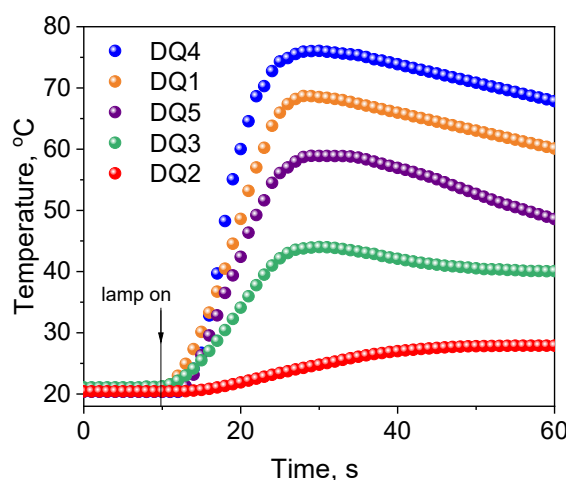


Figure 6. Kinetic curves of TMPTA polymerization photoinitiated by synthesized dyes in pair with electron donor—thiophenoxyacetic acid (0.1 M). The light intensity emitted by the dental lamp was 20 mW cm^{-2} .

Table 4. Initial rate of photoinitiated free radical polymerization of TMPTA initiated by photoredox pairs (R_p).

Co-Initiators	$R_p, \mu\text{mol}\cdot\text{s}^{-1}$					
	DQ1	DQ2	DQ3	DQ4	DQ5	CQ
PhTAA	109.06	6.25	42.59	115.30	77.22	144.10
PhTACA	74.64	4.46	29.17	76.77	48.20	87.33
DMA	80.86	4.77	15.59	71.97	51.48	99.30
PhIAA	88.80	5.72	23.92	91.39	47.37	92.96
PhAA	38.97	2.52	10.41	41.87	29.90	55.40
PhPA	58.45	4.03	15.92	62.81	43.95	78.66
MBX	125.68	7.12	50.25	131.27	88.03	164.27

Among the tested dyes, the most effective photoinitiators of TMPTA polymerization were DQ1 and DQ4. When designing the structures of these compounds, the need to generate a long-lived triplet state with high efficiency was taken into account, because via this state, radicals that initiate the photopolymerization reaction are effectively formed. The kinetic equations describing the photopolymerization rate [27] indicate that it depends, among other parameters, on the quantum yield of triplet state formation. Photocurable compositions containing a quinoline derivative (DQ2) have a poor ability to initiate the TMPTA polymerization process. Modification of its structure by introducing an additional nitrogen atom result in an increase in the quantum yield of the triplet state formation by as much as 90 times (DQ2 $\Phi_T = 0.006$ vs. DQ4 $\Phi_T = 0.54$), and thus an increase in the photopolymerization rate by approximately 20 times. However, indenoquinoxaline DQ5 has almost three times higher quantum yield of triplet state formation compared to indoloquinoxaline DQ3, which initiates the acrylate polymerization reaction less effectively. The introduction of an additional methyl group into the structure of the quinoxaline derivative (DQ3 vs. DQ4) results in an increase in the quantum yield of the triplet state formation by six times. The methyl group is an electron-donating substituent capable of donating non-bonding electrons to the conjugated double bond of the aromatic ring (partial charge transfer occurs from the carbon atom to the benzene ring). This causes the bathochrome effect observed in the long-wavelength band of the absorption spectrum (DQ3—386 nm, DQ4—405 nm). Therefore, DQ4 absorbs visible light more effectively. As a result, this dye has better photoinitiating abilities than DQ3.

Influence of Co-Initiator Structure

The data presented in Figures 6 and 7 and Table 4 confirm that the structure of the co-initiator has a decisive influence on the initial rate of TMPTA radical polymerization. The selection of electron donors was based on our many years of research on the photoinitiated polymerization process [19,23,29,57,58]. A thorough analysis of the presented results confirms that the presence of an oxygen atom in the electron donor structure (PhAA and PhPA) reduces the initial photopolymerization rate compared to co-initiators containing a sulfur atom (PhTAA and PhTACA) and a nitrogen atom (PhIAA and DMA). This is associated with a more efficient PET process and the different reactivity of radicals generated in secondary reactions following the electron transfer process. The following polymerization initiating radicals can be formed from the co-initiators: from phenoxyacetic acid— $\text{C}_6\text{H}_5\text{O}\dot{\text{C}}\text{HCOOH}$ and $\text{C}_6\text{H}_5\text{O}\dot{\text{C}}\text{H}_2$, from thiophenoxyacetic acid— $\text{C}_6\text{H}_5\text{S}\dot{\text{C}}\text{HCOOH}$ and $\text{C}_6\text{H}_5\text{S}\dot{\text{C}}\text{H}_2$ and from *N*-phenyliminodiacetic acid— $\text{C}_6\text{H}_5\text{NHC}(\text{COOH})_2$ and $\text{C}_6\text{H}_5\text{NH}\dot{\text{C}}\text{H}_2$ [58–62]. Analysis of the products obtained from *N,N*-dimethylaniline under photoreductive conditions indicates the presence of *N*-methylformanilide, *N*-methylaniline and trace amounts of other compounds [63], while thioanisole, thiophenol, CO_2 and diphenyldisulfide can be formed from thiophenoxyacetic acid [30,64]. Moreover, the decomposition of phenoxyacetic acid produces anisole, phenol, CO_2 and 1,2-diphenoxyethane [65,66],

while *N*-methyl-aniline, aniline, formanilide, CO₂, as well as dianilinomethane and *N*-methyleneaniline are obtained from *N*-phenyliminodiacetic acid [64–67].

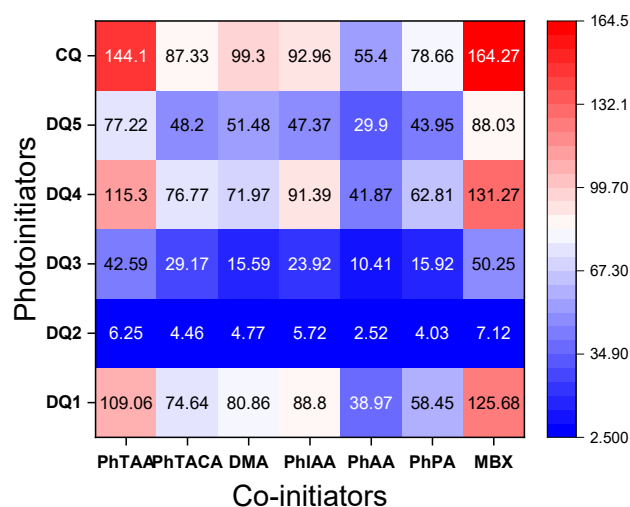


Figure 7. Heat maps of polymerization rates ($\mu\text{mol s}^{-1}$) obtained during photoinitiated polymerization using tested dyes and co-initiators (0.1 M). The light intensity of the dental lamp was 20 mW cm^{-2} .

The second carboxyl group present at the heteroatom is also responsible for the increase in the polymerization rate of TMPTA in systems containing PhIAA as an electron donor. This is confirmed by the fact that in the initiation mechanism based on carboxylic acids, after the electron transfer process, subsequent reactions involve proton transfer and decarboxylation, which lead to the formation of a radical initiating polymerization (Figure 5) [60]. Thus, the presence of two carboxyl groups in the electron donor molecule may lead to the formation of a diradical.

Furthermore, the analysis of the data collected in Table 4 and heat maps (Figure 7) shows that the synthesized dyes are effective photoinitiators of the polymerization reaction, also initiated by the hydrogen atom transfer mechanism. The photopolymerization rates obtained for light-cured compositions containing 2-mercaptobenzoxazole (MBX) as a hydrogen atom donor are comparable to those containing the electron donor PhTAA.

To sum up, the obtained quinoline and quinoxaline derivatives can be used as visible light photoinitiators in systems containing both electron donors and hydrogen atom donors as co-initiators. In the tested systems, radicals initiating TMPTA polymerization are formed as a result of intermolecular electron transfer, followed by the proton transfer between the components of the radical ion pair or decarboxylation depending on the solvent polarity. The second mechanism involves the hydrogen atom transfer from 2-mercaptobenzoxazole to the excited dye.

2.3.2. Control Tests Using Commercial Compounds

To verify the photoinitiating abilities of the tested systems (quinoline and quinoxaline derivatives (DQ1–DQ5)—co-initiators), the initial rates of free radical polymerization were determined and compared with the rate obtained for the system based on the commercial CQ photoinitiator used in dentistry (Figure 8). To conduct the experiment precisely, the same conditions were maintained, i.e., the number of absorbed photons. Therefore, the concentration of CQ (approx. 0.675 M) in the composition was approximately 500 times higher than that of the tested sensitizers due to the lower molar absorption coefficient in the visible region ($8 \text{ M}^{-1} \text{ cm}^{-1}$ vs. approximately $4000 \text{ M}^{-1} \text{ cm}^{-1}$ at 400 nm). As a result, thick polymer layers (3 mm) were obtained for the new systems, which do not contain significant amounts of unreacted photoinitiator and products formed during its decomposition.

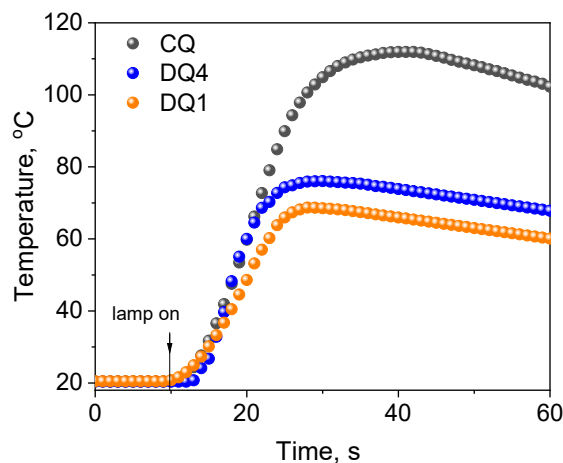


Figure 8. Comparison of the photoinitiating abilities of systems containing quinoline[2,3-*b*]-1*H*-imidazo[1,2-*a*]pyridinium bromide (DQ1) and 6-methyl-6*H*-indolo[2,3-*b*]quinoxaline (DQ4) as photoinitiator to camphorquinone (CQ). The tested photoinitiating systems have the same co-initiator (phenylthio)acetic acid (PhTAA). Kinetic curves were recorded during measurements of temperature changes during TMPTA polymerization photoinitiated by DQ1-PhTAA, DQ4-PhTAA and CQ-PhTAA pairs. The co-initiator concentration was 0.1 M and the light intensity of the dental lamp was 20 mW/cm².

Moreover, the temperature increases during polymerization photoinitiated by quinoline/quinoxaline derivative—thiophenoxyacetic acid systems was lower than for the commercial CQ photoinitiator, which is particularly important from the viewpoint of the potential application of these systems in dentistry. The data presented in Table 4 and Figure 8 clearly indicate that the initial TMPTA polymerization rates for systems containing DQ1 and DQ4 are similar to the data obtained for CQ. Hard polymer enamel is obtained after approximately 25 s of exposure (Figure 8).

2.3.3. Kinetic and Thermodynamic Conditions of the Polymerization Process

According to the kinetic equations describing the photopolymerization rate, the formation of radicals occurs in the triplet state of the photoinitiator. Considering this assumption, for the tested photoinitiating systems, the initial rate of photoinitiated TMPTA (R_p) polymerization should depend linearly on the square root of the quantum yield of triplet state formation. Based on the correlation shown in Figure 9, it can be concluded that the electron transfer process from the electron donor (PhTAA) to the photoinitiator (DQ1–DQ5) takes place in the excited triplet state.

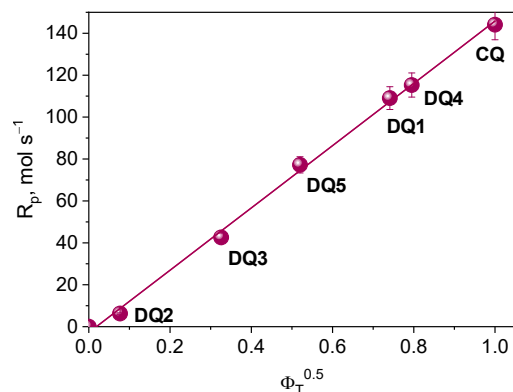


Figure 9. Dependence of the initial rate of photoinitiated TMPTA polymerization on the square root of the quantum yield of triplet state formation.

Figure 10 shows the dependence of the initial rate of photoinitiated TMPTA polymerization on the square root of the electron transfer rate constant. The observed linear correlation indicates that the process limiting the initial rate of free radical polymerization is the intermolecular electron transfer process.

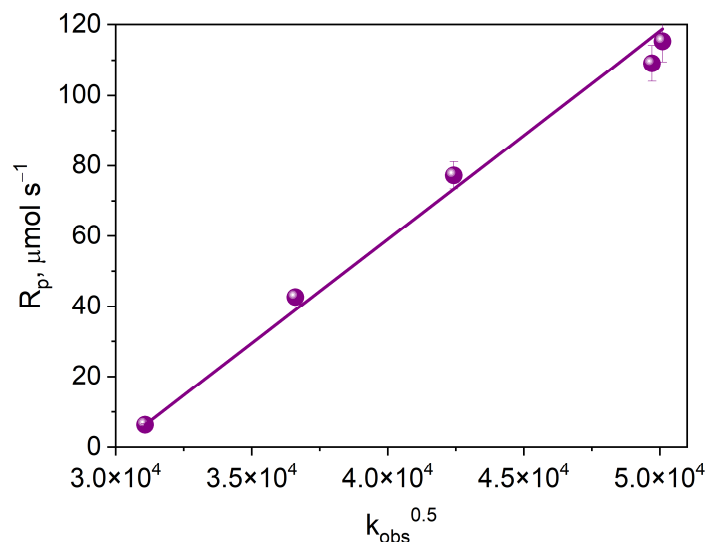


Figure 10. Dependence of the initial rate of photoinitiated TMPTA polymerization on the square root of the electron transfer rate constant.

Radical polymerization proceeding through the mechanism of intermolecular electron transfer is a multi-stage process, the main of which is the electron transfer from an electron donor molecule to an electron acceptor molecule in the excited state. The photoinduced electron transfer process is limited by thermodynamic factors, including the free energy of activation for the electron transfer process (PET), ΔG_{el} . The ΔG_{el} value can be determined experimentally using the Rehm–Weller equation [68,69]:

$$\Delta G_{el} = E_{ox} - E_{red} - \frac{Ze^2}{\epsilon a} - E_T^{00} \quad (3)$$

where: E_{ox} is the oxidation potential of the co-initiator, E_{red} is the reduction potential of the dye, E_T^{00} is the energy of the excited state (transition energy $T_1 \rightarrow S_0$)

To calculate the ΔG_{el} value, the oxidation potential of the co-initiator—PhTAA ($E_{ox} = 1.450$ V), the reduction potential of electron acceptors (Table 1) and the transition energy $T_1 \rightarrow S_0$ should be determined. The data are summarized in Table 1. The negative ΔG_{el} values indicate that the photoinduced electron transfer process is thermodynamically allowed.

According to Equation (4), if the intermolecular electron transfer process between the excited dye molecule and the electron donor molecule is a process limiting the polymerization rate, a parabolic relationship between the polymerization rate (R_p) and the free energy of activation (ΔG_{el}) for the PET process should be observed [27,70–72].

$$\ln R_p = A - \frac{(\lambda + \Delta G_{el})^2}{8\lambda RT} \quad (4)$$

where: A for the initial polymerization time is:

$$A = \ln k_p - 0.5 \ln k_t + 1.5 \ln [M] + 0.5 \ln I_A \quad (5)$$

where: k_p and k_t are the polymerization rate and chain termination constant, respectively, $[M]$ is the monomer concentration, I_A is the intensity of the absorbed light, λ is the energy

necessary to achieve the transition states of both the excited molecule and the solvent molecule. The correlation resulting from Equation (4) is shown in Figure 11.

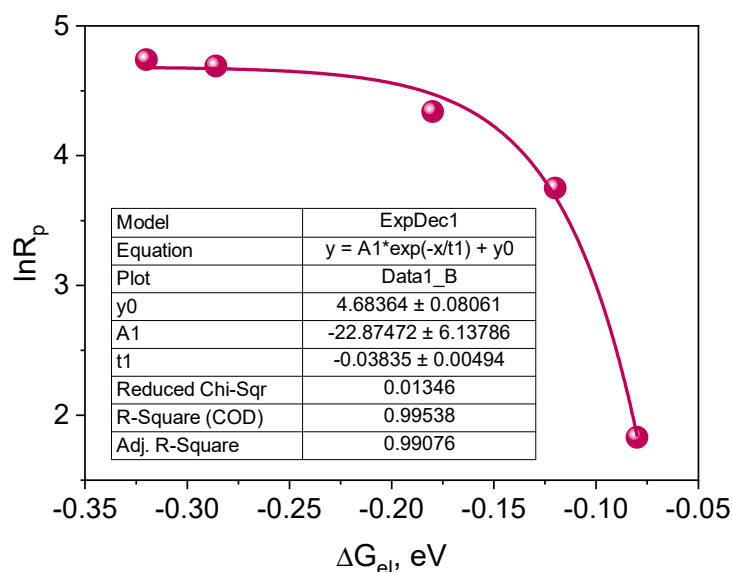


Figure 11. Dependence of the initial polymerization rate on the free energy of activation for the electron transfer process (PET) from the electron donor to the excited triplet state of the synthesized dyes.

The plot presented in Figure 11 indicates that the correlation between the initial polymerization rate and the free energy of activation for the electron transfer process (PET) is a fragment of a parabola. Therefore, it can be concluded that the tested photoredox pairs behave in accordance with the classical theory of the photoinduced electron transfer process [70,72]. The PET process is a rate-limiting polymerization process. Experimental points are located in the so-called normal Marcus area, i.e., the area in which the rate of the process increases as its driving force increases [27,70,72,73].

3. Materials and Methods

3.1. Reagents

Reagents for dye synthesis were purchased from Alfa Aesar Co., Ward Hill, MA, USA (ninhydrin, 1,2-diaminobenzene) and Merck, Rahway, NJ, USA (ethyl bromoacetate, 2-indolinone, isatin, 1-methylisatin, 2-aminopyridine, 2-aminobenzaldehyde). Solvents used either for synthesis or spectroscopic measurements, i.e., acetic acid, isopropanol, ethanol, methanol, ethyl acetate, 1-methyl-2-pyrrolidinone (MP), chloroform, deuterated chloroform (CDCl_3) and dimethyl sulfoxide ($\text{DMSO}-d_6$) were provided by Merck. Monomer, trimethylolpropane triacrylate (TMPTA), commercial photoinitiator, camphorquinone (CQ) and electron donors: (phenylthio)acetic acid (PhTAA), phenylacetic acid (PhAA), 2-phenylpropionic acid (PhPA), *N,N*-dimethylaniline (DMA), 3-(phenylthio)acrylic acid (PhTACA) and hydrogen donor 2-mercaptobenzoxazole (MBX) were obtained from Sigma-Aldrich Co., St. Louis, MO, USA while *N*-phenyliminodiacetic acid (PhIAA) was from Lancaster, Kenilworth, NJ, USA. Thin layer chromatography plates (DC-Plastikfolien Silica gel 60 F254, 0.2 mm) from Merck Co. Rahway, NJ, USA.

The structures of the co-initiators used are shown in Figure 12. They are divided into two groups, i.e., electron donors and hydrogen atom donors.

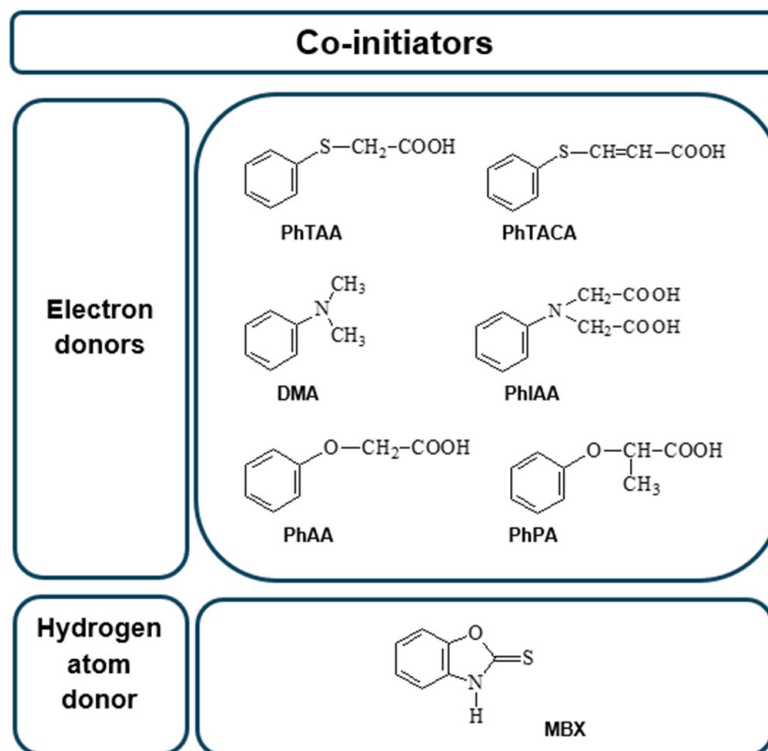


Figure 12. Structures of co-initiators used in the photoinitiating composition.

3.2. Synthesis

The dyes were synthesized by the reactions shown in Figures 13 and 14. The methods for synthesizing the tested compounds described in this work, although based on literature data, have been modified and improved for simplicity. The available literature describes their syntheses based on other reagents or other solvents with different yields [74,75]. In some cases, other techniques were also used, e.g., microwave [76,77].

For example, the synthesis of the DQ1 dye reported by us has not been described in the literature. In Van Dormael's work [78], only the first stage of the synthesis is described, leading to the intermediate product 2-oxo-2,3-dihydro-1*H*-imidazo[1,2-*a*]pyridinium bromide. Moreover, the author proposes carrying out the reaction without adding a solvent. Due to the high exothermicity of this process, it is very troublesome. Therefore, we tested a large group of solvents and found that the reaction was most effective with the addition of 2-propanol. Moreover, unlike the work we published in *Polymer* in 2007 [79], the second stage of the synthesis was completely refined and shortened. In a previous work [79], 2-oxo-2,3-dihydro-1*H*-imidazo[1,2-*a*]pyridinium bromide was used as an intermediate, which was condensed with 2-nitrobenzaldehyde and then reduced with iron. Unfortunately, the final product was obtained with unsatisfactory yield. In this work, 2-aminobenzaldehyde was used as a reagent, which in the presence of glacial acetic acid very easily condenses with 2-oxo-2,3-dihydro-1*H*-imidazo[1,2-*a*]pyridinium bromide to give the desired compounds. The developed method of synthesizing the tested compounds (DQ1–DQ5) using glacial acetic acid as a solvent is very simple. The reaction is carried out under reflux at normal pressure without the use of microwaves and the products are obtained in good yields.

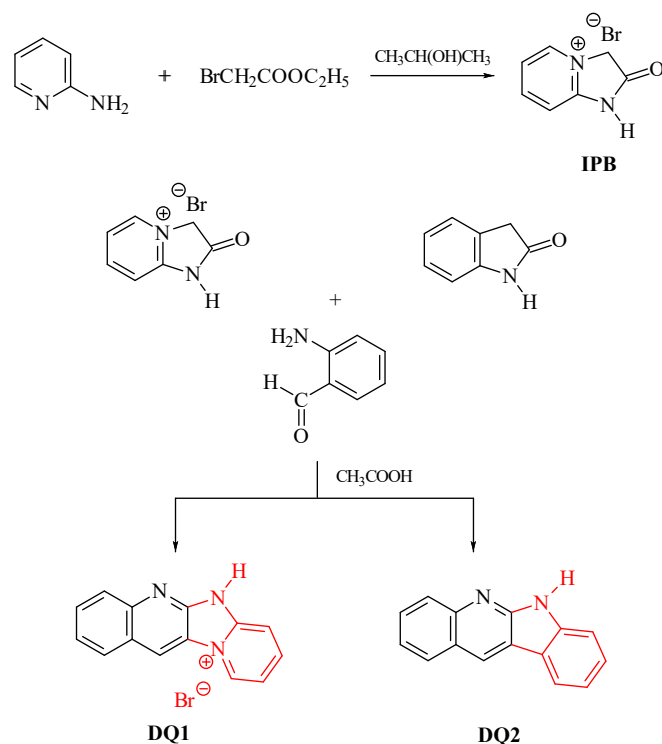


Figure 13. Synthesis of quinoline derivatives DQ1–DQ2; red color indicates the main modification of the dye structure.

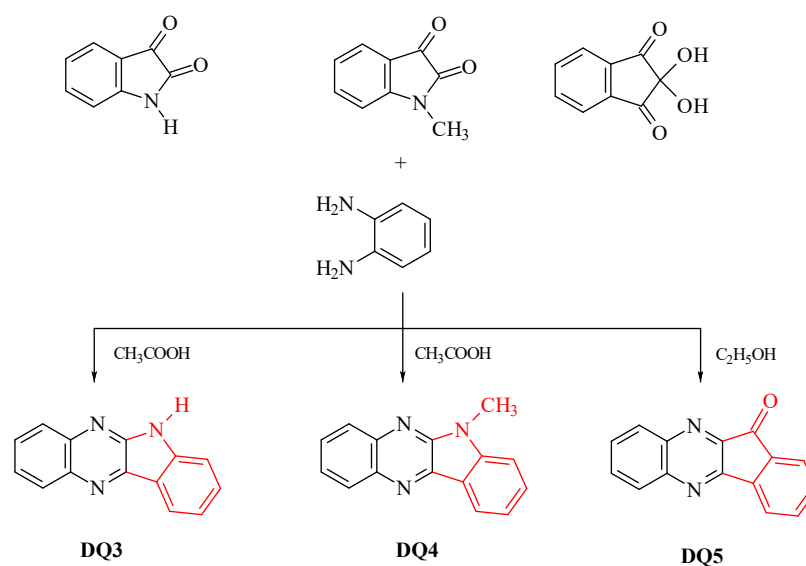


Figure 14. Synthesis of quinoxaline derivatives DQ3–DQ5; red color indicates the main modification of the dye structure.

The progress of the reactions was monitored by thin-layer chromatography on silica gel 60F 254 using chloroform:methanol (9:1 *v/v*) (DQ1, DQ2, DQ3, DQ4) and chloroform (DQ5) as an eluent. The products were identified spectroscopically. The ^1H and ^{13}C NMR spectra are shown as images before Figure S1 in Supplementary Materials.

DQ1: Quinoline[2,3-*b*]-1*H*-imidazo[1,2-*a*]pyridinium bromide

The dye quinoline[2,3-*b*]-1*H*-imidazo[1,2-*a*]pyridinium bromide (DQ1) was obtained in a two-step reaction according to the following procedure.

Step 1: 2-oxo-2,3-dihydro-1*H*-imidazo[1,2-*a*]pyridinium bromide (IPB)

In the first stage, to obtain an intermediate product—2-oxo-2,3-dihydro-1*H*-imidazo[1,2-*a*]pyridinium bromide (IPB), 4.7 g (0.05 mol) 2-aminopyridine and 25 mL of 2-propanol. At a boiling point of approximately 82 °C, 6.2 g (0.05 mol) of ethyl chloroacetate were added dropwise. After complete addition of ethyl bromoacetate, the reaction mixture was heated for approximately 30 min. The separated precipitate of 2-oxo-2,3-dihydro-1*H*-imidazo[1,2-*a*]pyridinium bromide was filtered and then washed twice with 5 mL of acetone. The obtained product was crystallized from 40 mL of methanol to obtain 3.5 g (45%) of crystals, C₇H₇N₂OBr, 215.04 g/mol, m.p. 230–232 °C [78,79].

¹H NMR (400 MHz, DMSO-*d*₆) δ (ppm): 8.80–8.77 (d, ³J_{H,H} = 8.0 Hz, 1H), 8.44–8.35 (t, 1H), 7.60–7.59 (d, ³J_{H,H} = 8.0 Hz, 1H), 7.57–7.52 (t, 1H), 5.29 (s, 2H, CH₂).

¹³C NMR (200 MHz, DMSO-*d*₆) δ (ppm): 169.6, 153.3, 147.0, 139.4, 118.8, 110.7, 55.3.

Step 2

In the second stage, 2.15 g (0.01 mol) of 2-oxo-2,3-dihydro-1*H*-imidazo[1,2-*a*]pyridinium bromide and 50 mL of glacial acetic acid were introduced into a round-bottomed flask equipped with a reflux condenser and a stirrer. The mixture was stirred and 1.21 g (0.01 mol) of 2-aminobenzaldehyde was added at room temperature. The reaction mixture was heated at reflux for 3 h to give 2.04 g (68%) of crystals. The obtained product was crystallized from 50 mL of methanol, C₁₃H₁₀N₃Br, 300.15 g/mol, m.p. 264–265 °C [78,79].

¹H NMR (400 MHz, DMSO-*d*₆) δ (ppm): 7.11–7.15 (d, ³J_{H,H} = 8.0 Hz, 1H), 7.28–7.35 (t, 1H), 7.38–7.46 (t, 1H), 7.89–7.93 (d, ³J_{H,H} = 8.0 Hz, 1H), 8.00–8.03 (d, ³J_{H,H} = 8.0 Hz, 1H), 8.14–8.18 (t, 1H), 8.25–8.29 (d, ³J_{H,H} = 8.0 Hz, 1H), 8.53 (s, 1H), 9.40–9.58 (t, 1H), 12.55(NH, 1H).

¹³C NMR (200 MHz, DMSO-*d*₆) δ (ppm): 152.1, 148.9, 140.6, 132.8, 130.8, 129.7, 126.1, 125.8, 124.3, 122.4, 122.3, 115.4, 115.1.

DQ2; 6*H*-indolo[2,3-*b*]quinoline

6*H*-indolo[2,3-*b*]quinoline (DQ2) was obtained by refluxing 1.33 g (0.01 mol) 2-indolinone with 1.21 g (0.01 mol) 2-aminobenzaldehyde in the presence of glacial acetic acid (40 mL). The isolated product was crystallized from a 1:1 *v/v* mixture of dimethylformamide and ethanol to obtain 1.72 g (79%) of light yellow crystals, C₁₅H₁₀N₂, 218.25 g/mol, m.p. 342–345 °C [80,81].

¹H NMR (400 MHz, DMSO-*d*₆) δ (ppm): 11.68 (s, 1H), 9.04 (s, 1H), 8.27–8.23 (d, ³J_{H,H} = 8.0 Hz, 1H), 8.12–8.07 (d, ³J_{H,H} = 8.0 Hz, 1H), 7.98–7.94 (d, ³J_{H,H} = 8.0 Hz, 1H), 7.50–7.55 (t, 1H), 7.52–7.42 (m, 3H), 7.29–7.21 (t, 1H).

¹³C NMR (200 MHz, DMSO-*d*₆) δ (ppm): 146.3, 144.4, 140.6, 140.2, 139.0, 131.7, 129.5, 129.2, 127.95, 126.4, 122.7, 121.1, 119.4, 112.4.

DQ3; 6*H*-indolo[2,3-*b*]quinoxaline

6*H*-indolo[2,3-*b*]quinoxaline (DQ3) was obtained by refluxing (approx. 1 h) 1.47 g (0.01 mol) isatin with 1.08 g (0.01 mol) 1,2-diaminobenzene in glacial acetic acid (60 mL). The isolated product was crystallized from a mixture of dimethylformamide and ethanol (1:1 *v/v*) to obtain 1.65 g (75%) of light yellow crystals, C₁₄H₉N₃, 219.24 g/mol, m.p. 297–298 °C [74,82–84].

¹H NMR (400 MHz, DMSO-*d*₆) δ (ppm): 12.05 (s, 1H), 8.35–8.37 (d, ³J_{H,H} = 8.0 Hz, 1H), 8.25–8.27 (m, 1H), 8.07–8.09 (m, 1H), 7.79–7.83 (m, 1H), 7.70–7.75 (m, 2H), 7.58–7.60 (d, ³J_{H,H} = 8.0 Hz, 1H), 7.36–7.40 (m, 1H).

¹³C NMR (200 MHz, DMSO-*d*₆) δ (ppm): 146.3, 144.4, 140.6, 140.2, 139.0, 131.7, 129.5, 129.2, 127.9, 126.4, 122.7, 121.1, 119.4, 112.4.

DQ4; 6-methyl-6*H*-indolo[2,3-*b*]quinoxaline

6-methyl-6*H*-indolo[2,3-*b*]quinoxaline (DQ4) was prepared by refluxing 1.61 g (0.01 mol) 1-methylisatin with 1.08 g (0.01 mol) 1,2-diaminobenzene in glacial acid vinegar (60 mL). The isolated product was crystallized from a mixture of dimethylformamide and ethanol (1:1 *v/v*) to obtain 1.88 g (81%) of light yellow crystals, C₁₅H₁₁N₃, 233.26 g/mol, m.p. 146–147 °C [82,85,86].

^1H NMR (400 MHz, CDCl_3) δ (ppm): 8.52–8.48 (d, $^3J_{\text{H,H}} = 8.0$ Hz, 1H), 8.34–8.30 (d, $^3J_{\text{H,H}} = 8.0$ Hz, 1H), 8.18–8.13 (d, $^3J_{\text{H,H}} = 8.0$ Hz, 1H), 7.78–7.69 (m, 3H), 7.51–7.41 (m, 1H), 7.37–7.26 (m, 1H), 4.03 (CH_3 , 3H).

^{13}C NMR (200 MHz, CDCl_3) δ (ppm): 145.9, 145.4, 140.7, 140.3, 132.1, 131.0, 129.3, 127.7, 127.5, 126.8, 122.1, 121.5, 110.3, 109.4, 27.8.

DQ5; 11*H*-indeno[1,2-*b*]quinoxalin-11-on

11*H*-indeno[1,2-*b*]quinoxalin-11-one (DQ5) was prepared by refluxing 1.78 g (0.01 mol) ninhydrin with 1.08 g (0.01 mol) 1,2-diaminobenzene in ethanol (50 mL). Three drops of acetic acid were added to the reaction mixture and heated at reflux for 3 h. The isolated product was crystallized from dimethylformamide to obtain 2.10 g (91%) of light yellow crystals, $\text{C}_{15}\text{H}_8\text{N}_2\text{O}$, 232.24 g/mol, m.p. 224–225 °C [82,85,86].

^1H NMR (400 MHz, $\text{DMSO}-d_6$) δ (ppm): 8.20–8.14 (t, 2H), 8.11–8.09 (d, $^3J_{\text{H,H}} = 8$ Hz, 1H), 7.95–7.84 (m, 4H), 7.74–7.70 (t, 1H).

^{13}C NMR (200 MHz, $\text{DMSO}-d_6$) δ (ppm): 189.8, 156.9, 150.3, 142.6, 142.3, 141.5, 137.4, 137.1, 133.2, 132.9, 131.4, 130.8, 129.8, 124.7, 122.7.

3.3. Methods

Electronic absorption spectra were recorded on a Shimadzu UV-Vis Multispec-1501 spectrophotometer, Kyoto, Japan, in ethyl acetate solution. Electronic emission spectra were recorded on a Hitachi F-4500 spectrophotometer, Tokio, Japan. Fluorescence spectra were recorded at room temperature in 2-methyltetrahydrofuran. The fluorescence quantum yield was determined by a comparative method using a solution of 9-methylanthracene [41] in 2-methyltetrahydrofuran as a standard. Phosphorescence spectra were recorded in 2-methyltetrahydrofuran at liquid nitrogen temperature.

The reduction potentials of the synthesized dyes were determined in a 0.1 M solution of tetrabutylammonium perchlorate in anhydrous acetonitrile, based on cyclic voltammograms recorded on an MTM Model EA9C-4z cyclovoltammeter, Electroanalytical MTM System (Krakow) Model EA9C-4z, EA, Krakow, Poland. A platinum disk electrode was used as the working electrode and a platinum wire and an Ag/AgCl electrode were used as the auxiliary and reference electrodes, respectively.

The kinetics of photoinitiated polymerization was studied using the microcalorimetric method [30,35,87]. The polymerizing compositions contained 0.9 g of TMPTA as monomer, 0.1 mL of 1-methyl-2-pyrrolidone (MP), from 1.35×10^{-3} to 1.8×10^{-3} M (depending on the molar absorption coefficient) of synthesized dyes as photoinitiators (electron acceptors) and 0.1 M of an electron donor as a co-initiator. The reference formulation did not contain an electron donor. The photocurable composition was placed in a Teflon ring with a diameter of 10 mm and a thickness of 3 mm, protected on one side with a glass plate. A thermocouple (stainless steel, type K, $\Phi 4$ mm, RTD Thermometer Delta OHM HD 2107.1, Delta OHM, Padova, Italy) was placed in it from the top so that its tip was in contact with the surface of the glass plate. The sample was irradiated through the bottom glass plate with blue light from a dental LED lamp (Cromalux 75 Mega Physik Dental, 390–500 nm, MEGA-PHYSIK GMBH & CO, Rastatt, Germany). Its intensity was checked with a Coherent Field Master meter and amounted to 20 mW/cm². The distance of the sample from the light source was the same for all measurements. The time needed to stabilize the temperature in the sample before irradiation was 10 s and was the same for all experiments. Temperature changes during the polymerization process were recorded every 1 s with an accuracy of ± 0.1 °C using a recorder (Delta OHM HD 40.1, Padova, Italy) connected to a thermocouple. Three measurements were performed for each of the tested materials. A commercial photoinitiator—camphorquinone (CQ) was used to assess the effectiveness of initiating the polymerization reaction by the tested systems. Its concentration was 0.675 M.

The lifetime of the excited triplet state of the synthesized dyes was determined in acetonitrile based on transient absorption spectra recorded on nanosecond laser flash photolysis using an LSK 60 Laser Flash Photolytics camera (Applied Photophysics, Leatherhead, UK). A pulsed laser emitting radiation with a wavelength of 355 nm from Lambda

Phisik/model LPY 150, Saxonburg, PA, USA) was used to excite the sample. The energy of the laser pulses was 65 mJ.

4. Conclusions

The paper focused on two-component photoinitiating systems based on quinoline and quinoxaline dyes combined with acetic acid derivatives for application in dental filling materials. To obtain effective photoinitiators operating in the visible region, the parent structure of quinoline (DQ2) was modified to the quinoxaline derivatives. Therefore, the synthesized compounds differ in the number of nitrogen atoms (DQ1–DQ5), the presence of a methyl substituent (DQ4), or an oxygen atom (DQ5). Their full spectral characteristics based on NMR, UV-Vis, fluorescence and phosphorescence, along with a description of their synthesis, are presented. The electronic absorption spectra of these dyes are characterized by an intense absorption band located in the range of 320–350 nm and a second, less intense absorption band shifted by ca. 35–50 nm to the red. The results of steady-state and time-resolved spectroscopic studies confirm the formation of the triplet state by the tested dyes. Based on the recorded transient absorption spectra, the lifetime and quantum yield of the triplet state were determined. The revealed physicochemical properties of the tested dyes allowed their use as initiators in compositions photoinitiated with light emitted by a dental lamp.

These compounds turned out to be effective photoinitiators of free radical polymerization of TMPTA in the visible light range, induced by dental lamp light in the presence of an electron donor or a hydrogen atom. Good photoinitiation abilities have been confirmed by comparative tests with systems containing a commercial photoinitiator used in dentistry—camphorquinone (CQ). Two of the obtained compounds, a quinoline derivative (DQ1) and a quinoxaline derivative (DQ4), used in light-cured compositions, indicate similar values of the initial photopolymerization rate of acrylates to the data obtained for CQ. The high rate of the chain reaction and short polymerization time confirm that the new two-component initiating systems can be used in much lower concentrations, without slowing down the speed of obtaining polymer materials.

Supplementary Materials: The following supporting information can be downloaded at: <https://www.mdpi.com/article/10.3390/ijms25084289/s1>.

Author Contributions: Conceptualization, I.P.; Methodology, I.P.; Formal analysis, B.J.; Investigation, I.P.; Data curation, I.P. Writing—original draft, I.P.; Writing—review & editing, B.J.; Visualization, I.P. and B.J.; Supervision, B.J. All authors have read and agreed to the published version of the manuscript.

Funding: This research received no external funding.

Institutional Review Board Statement: Not applicable.

Informed Consent Statement: Not applicable.

Data Availability Statement: The data are not publicly available apart from the data contained in the article or Supplementary Materials.

Conflicts of Interest: The authors declare no conflicts of interest.

References

1. Sharm El-Sheikh Climate Change Conference, Sharm El-Sheikh, Egypt, 6–20 November 2022. Available online: <https://unfccc.int/cop27> (accessed on 5 November 2022).
2. Liang, M.; Borjigin, T.; Zhang, Y.; Liu, H.; Liu, B.; Guo, H. Z-Scheme Au@Void@g-C₃N₄/SnS Yolk–Shell Heterostructures for Superior Photocatalytic CO₂ Reduction under Visible Light. *ACS Appl. Mater. Interfaces* **2018**, *10*, 34123–34131. [[CrossRef](#)]
3. Billerbeck, K.; Hägele, C.; Träger, J. Relation of the Working Curve and Exposure Intensity in VPP 3D-Printing. *Prog. Addit. Manuf.* **2023**, *2*, 1–9. [[CrossRef](#)]
4. de Oliveira, E.R.M.; Vieira, R.P. Synthesis and Characterization of Poly(Limonene) by Photoinduced Controlled Radical Polymerization. *J. Polym. Environ.* **2020**, *28*, 2931–2938. [[CrossRef](#)]
5. Tawagi, E.; Ganesh, T.; Cheng, H.-L.M.; Santerre, J.P. Synthesis of Degradable-Polar-Hydrophobic-Ionic Co-Polymeric Microspheres by Membrane Emulsion Photopolymerization: In Vitro and in Vivo Studies. *Acta Biomater.* **2019**, *89*, 279–288. [[CrossRef](#)]

6. Messaddeq, S.H.; Bonnet, A.-S.; Santagnelli, S.H.; Salek, G.; Colmenares, Y.N.; Messaddeq, Y. Photopolymerized Hybrids Containing TiO₂ Nanoparticles for Gradient-Index Lens. *Mater. Chem. Phys.* **2019**, *236*, 121793. [[CrossRef](#)]
7. Wei, L.; Shang, S.; Zheng, Y.; Liu, J.; Zhu, P. Iridescent Structural Colors Printing on Cellulose Fabrics with Robust Structural Coloration. *Dye. Pigment.* **2024**, *221*, 111824. [[CrossRef](#)]
8. Dumur, F. Recent Advances on Phenothiazine-Based Oxime Esters as Visible Light Photoinitiators of Polymerization. *Eur. Polym. J.* **2024**, *202*, 112597. [[CrossRef](#)]
9. Dumur, F. The Future of Visible Light Photoinitiators of Polymerization for Photocrosslinking Applications. *Eur. Polym. J.* **2023**, *187*, 111883. [[CrossRef](#)]
10. Dumur, F. Recent Advances on Carbazole-Based Photoinitiators of Polymerization. *Eur. Polym. J.* **2020**, *125*, 109503. [[CrossRef](#)]
11. Ma, Q.; Zhang, Y.; Launay, V.; Le Dot, M.; Liu, S.; Lalevée, J. How to Overcome the Light Penetration Issue in Photopolymerization? An Example for the Preparation of High Content Iron-Containing Opaque Composites and Application in 3D Printing. *Eur. Polym. J.* **2022**, *165*, 111011. [[CrossRef](#)]
12. Lalevee, J.; Fouassier, J.P. *Dyes and Chromophores in Polymer Science*; ISTE Ltd.; John Wiley & Sons Inc.: Hoboken, NJ, USA, 2015.
13. Jasinski, F.; Zetterlund, P.B.; Braun, A.M.; Chemtob, A. Photopolymerization in Dispersed Systems. *Prog. Polym. Sci.* **2018**, *84*, 47–88. [[CrossRef](#)]
14. Dickens, S.H.; Stansbury, J.W.; Choi, K.M.; Floyd, C.J.E. Photopolymerization Kinetics of Methacrylate Dental Resins. *Macromolecules* **2003**, *36*, 6043–6053. [[CrossRef](#)]
15. Noè, C.; Hakkarainen, M.; Sangermano, M. Cationic UV-Curing of Epoxidized Biobased Resins. *Polymers* **2021**, *13*, 89. [[CrossRef](#)] [[PubMed](#)]
16. Dikova, T.; Maximov, J.; Todorov, V.; Georgiev, G.; Panov, V. Optimization of Photopolymerization Process of Dental Composites. *Processes* **2021**, *9*, 779. [[CrossRef](#)]
17. Andreu, A.; Su, P.-C.; Kim, J.-H.; Ng, C.S.; Kim, S.; Kim, I.; Lee, J.; Noh, J.; Subramanian, A.S.; Yoon, Y.-J. 4D Printing Materials for Vat Photopolymerization. *Addit. Manuf.* **2021**, *44*, 102024. [[CrossRef](#)]
18. Tomal, W.; Kiliclar, H.C.; Fiedor, P.; Ortyl, J.; Yagci, Y. Visible Light Induced High Resolution and Swift 3D Printing System by Halogen Atom Transfer. *Macromol. Rapid Commun.* **2023**, *44*, 2200661. [[CrossRef](#)] [[PubMed](#)]
19. Chen, H.; Noirbent, G.; Zhang, Y.; Sun, K.; Liu, S.; Brunel, D.; Gimes, D.; Graff, B.; Morlet-Savary, F.; Xiao, P.; et al. Photopolymerization and 3D/4D Applications Using Newly Developed Dyes: Search around the Natural Chalcone Scaffold in Photoinitiating Systems. *Dye. Pigment.* **2021**, *188*, 109213. [[CrossRef](#)]
20. Bonardi, A.H.; Dumur, F.; Grant, T.M.; Noirbent, G.; Gimes, D.; Lessard, B.H.; Fouassier, J.-P.; Lalevée, J. High Performance Near-Infrared (NIR) Photoinitiating Systems Operating under Low Light Intensity and in the Presence of Oxygen. *Macromolecules* **2018**, *51*, 1314–1324. [[CrossRef](#)]
21. Corrigan, N.; Yeow, J.; Judzewitsch, P.; Xu, J.; Boyer, C. Seeing the Light: Advancing Materials Chemistry through Photopolymerization. *Angew. Chem. Int. Ed.* **2019**, *58*, 5170–5189. [[CrossRef](#)]
22. Lalevée, J.; Allonas, X.; Jradi, S.; Fouassier, J.-P. Role of the Medium on the Reactivity of Cleavable Photoinitiators in Photopolymerization Reactions. *Macromolecules* **2006**, *39*, 1872–1879. [[CrossRef](#)]
23. Yagci, Y.; Jockusch, S.; Turro, N.J. Photoinitiated Polymerization: Advances, Challenges, and Opportunities. *Macromolecules* **2010**, *43*, 6245–6260. [[CrossRef](#)]
24. Paczkowski, J.; Neckers, D.C. Photoinduced Electron Transfer Initiating Systems for Free-Radical Polymerization. In *Electron Transfer in Chemistry*; Wiley: Hoboken, NJ, USA, 2008; Volume 5.
25. Zhang, J.; Zivic, N.; Dumur, F.; Xiao, P.; Graff, B.; Gimes, D.; Fouassier, J.P.; Lalevée, J. A Benzophenone-Naphthalimide Derivative as Versatile Photoinitiator of Polymerization under near UV and Visible Lights. *J. Polym. Sci. Part A Polym. Chem.* **2015**, *53*, 445–451. [[CrossRef](#)]
26. Lalevée, J.; Telitel, S.; Tehfe, M.A.; Fouassier, J.P.; Curran, D.P.; Lacôte, E. N-Heterocyclic Carbene Boranes Accelerate Type I Radical Photopolymerizations and Overcome Oxygen Inhibition. *Angew. Chem. Int. Ed.* **2012**, *51*, 5958–5961. [[CrossRef](#)] [[PubMed](#)]
27. Andrzejewska, E. Photopolymerization kinetics of multifunctional monomers. *Prog. Polym. Sci.* **2001**, *26*, 605–665. [[CrossRef](#)]
28. Wrzyszczyński, A.; Bartoszewicz, J.; Hug, G.L.; Marciniak, B.; Paczkowski, J. Photochemical Studies of a Photodissociative Initiator Based on a Benzophenone Derivative Possessing a Thioether Moiety. *J. Photochem. Photobiol. A Chem.* **2003**, *155*, 253–259. [[CrossRef](#)]
29. Pyszka, I.; Jędrzejewska, B. Photoinitiation Abilities of Indeno- and Indoloquinoxaline Derivatives and Mechanical Properties of Dental Fillings Based on Multifunctional Acrylic Monomers and Glass Ionomer. *Polymer* **2023**, *266*, 125625. [[CrossRef](#)]
30. Pyszka, I.; Jędrzejewska, B. Acenaphthoquinoxaline Derivatives as Dental Photoinitiators of Acrylates Polymerization. *Materials* **2021**, *14*, 4881. [[CrossRef](#)] [[PubMed](#)]
31. Kucybała, Z.; Wrzyszczyński, A. Photolysis of N-[(4-Benzoyl)Benzenesulfonyl]Benzenesulfonamide. *J. Photochem. Photobiol. A Chem.* **2002**, *153*, 109–112. [[CrossRef](#)]
32. Fouassier, J.P.; Allonas, X.; Burget, D. Photopolymerization Reactions under Visible Lights: Principle, Mechanisms and Examples of Applications. *Prog. Org. Coat.* **2003**, *47*, 16–36. [[CrossRef](#)]
33. Kabatc, J.; Kucybała, Z.; Pietrzak, M.; Ścigalski, F.; Paczkowski, J. Free Radical Polymerization Initiated via Photoinduced Intermolecular Electron Transfer Process: Kinetic Study 3. *Polymer* **1999**, *40*, 735–745. [[CrossRef](#)]

34. Jędrzejewska, B.; Wejnerowska, G. Highly Effective Sensitizers Based on Merocyanine Dyes for Visible Light Initiated Radical Polymerization. *Polymers* **2020**, *12*, 1242. [[CrossRef](#)] [[PubMed](#)]
35. Pyszka, I.; Kucybała, Z.; Jędrzejewska, B. Effective Singlet Oxygen Sensitizers Based on the Phenazine Skeleton as Efficient Light Absorbers in Dye Photoinitiating Systems for Radical Polymerization of Acrylates. *Materials* **2021**, *14*, 3085. [[CrossRef](#)] [[PubMed](#)]
36. Jędrzejewska, B.; Ośmiałowski, B. Difluoroboranyl Derivatives as Efficient Panchromatic Photoinitiators in Radical Polymerization Reactions. *Polym. Bull.* **2018**, *75*, 3267–3281. [[CrossRef](#)]
37. Strzelczyk, R.; Podsiadły, R. Naphthoylenebenzimidazolone Dyes as One-Component Photoinitiators. *Color. Technol.* **2017**, *133*, 178–183. [[CrossRef](#)]
38. Kabatc, J. The Influence of a Radical Structure on the Kinetics of Photopolymerization. *J. Polym. Sci. Part A Polym. Chem.* **2017**, *55*, 1575–1589. [[CrossRef](#)]
39. Balcerak, A.; Kabatc, J. The Photooxidative Sensitization of Bis(p-Substituted Diphenyl)Iodonium Salts in the Radical Polymerization of Acrylates. *RSC Adv.* **2019**, *9*, 28490–28499. [[CrossRef](#)] [[PubMed](#)]
40. Mousawi, A.A.; Dietlin, C.; Graff, B.; Morlet-Savary, F.; Toufaily, J.; Hamieh, T.; Fouassier, J.P.; Chachaj-Brekiesz, A.; Ortyl, J.; Lalevé, J. Meta-Terphenyl Derivative/Iodonium Salt/9H-Carbazole-9-Ethanol Photoinitiating Systems for Free Radical Promoted Cationic Polymerization upon Visible Lights. *Macromol. Chem. Phys.* **2016**, *217*, 1955–1965. [[CrossRef](#)]
41. Pyszka, I.; Kucybała, Z.; Pączkowski, J. Reinvestigation of the Mechanism of the Free Radical Polymerization Photoinitiation Process by Camphorquinone–Coinitiator Systems: New Results. *Macromol. Chem. Phys.* **2004**, *205*, 2371–2375. [[CrossRef](#)]
42. Allen, N.S. *Photochemistry and Photophysics of Polymer Materials*; Wiley: Hoboken, NJ, USA, 2010.
43. Borjigin, T.; Schmitt, M.; Giacometto, N.; Rico, A.; Bidotti, H.; Nechab, M.; Zhang, Y.; Graff, B.; Morlet-Savary, F.; Xiao, P.; et al. The Blue-LED-Sensitive Naphthoquinone-Imidazolyl Derivatives as Type II Photoinitiators of Free Radical Photopolymerization. *Adv. Mater. Interfaces* **2023**, *10*, 2202352. [[CrossRef](#)]
44. Kucková, L.; Jomová, K.; Švorcová, A.; Valko, M.; Segl'a, P.; Moncol, J.; Kožíšek, J. Synthesis, Crystal Structure, Spectroscopic Properties and Potential Biological Activities of Salicylate–Neocuproine Ternary Copper(II) Complexes. *Molecules* **2015**, *20*, 2115–2137. [[CrossRef](#)]
45. Abu Ali, H.; Abu Shamma, A.; Kamel, S. New Mixed Ligand Cobalt(II/III) Complexes Based on the Drug Sodium Valproate and Bioactive Nitrogen-Donor Ligands. Synthesis, Structure and Biological Properties. *J. Mol. Struct.* **2017**, *1142*, 40–47. [[CrossRef](#)]
46. Dhumwad, S.D. Synthesis, Characterization and Biological Studies of Co(II), Ni(II), Cu(II) and Zn(II) Complexes of Schiff Bases Derived from 3-Formyl-2-Mercaptoquinolines. *J. Chem. Pharm. Res.* **2011**, *3*, 504–517.
47. Jaman, Z.; Karim, M.R.; Siddiquee, T.A.; Mirza, A.H.; Ali, M.A. Synthesis of 5-Substituted 2, 9-Dimethyl-1,10-Phenanthroline Dialdehydes and Their Schiff Bases with Sulfur-Containing Amines. *Int. J. Org. Chem.* **2013**, *3*, 214–219. [[CrossRef](#)]
48. Abu Ali, H.; Kamel, S.; Abu Shamma, A. Novel Structures of Zn(II) Biometal Cation with the Biologically Active Substituted Acetic Acid and Nitrogen Donor Ligands: Synthesis, Spectral, Phosphate Diester Catalytic Hydrolysis and Anti-Microbial Studies. *Appl. Organomet. Chem.* **2017**, *31*, e3829. [[CrossRef](#)]
49. Jabali, B.; Abu Ali, H. New Zinc(II) Complexes of the Non-Steroidal Anti-Inflammatory Drug (Indomethacin) and Various Nitrogen Donor Ligands. Synthesis, Characterization and Biological Activity. *Polyhedron* **2016**, *117*, 249–258. [[CrossRef](#)]
50. Pereira, J.A.; Pessoa, A.M.; Cordeiro, M.N.D.S.; Fernandes, R.; Prudêncio, C.; Noronha, J.P.; Vieira, M. Quinoxaline, Its Derivatives and Applications: A State of the Art Review. *Eur. J. Med. Chem.* **2015**, *97*, 664–672. [[CrossRef](#)]
51. Segoviano-Garfias, J.J.N.; Zanon, G.A.; Ávila-Ramos, F.; Bivián-Castro, E.Y. Equilibrium Studies of Iron (III) Complexes with Either Pyrazine, Quinoxaline, or Phenazine and Their Catecholase Activity in Methanol. *Molecules* **2022**, *27*, 3257. [[CrossRef](#)]
52. Murov, S.L.; Carmichael, I.; Hug, G.L. *Handbook of Photochemistry*; Marcel Dekker: New York, NY, USA, 1993.
53. Lament, B.; Karpiuk, J.; Waluk, J. Determination of Triplet Formation Efficiency from Kinetic Profiles of the Ground State Recovery. *Photochem. Photobiol. Sci.* **2003**, *2*, 267–272. [[CrossRef](#)] [[PubMed](#)]
54. Stern, O.; Volmer, M. Über Die Abklingungszeit Der Fluoreszenz. *Physik. Zeitschr.* **1919**, *20*, 183–188.
55. Ghorbani, F.; Harry, S.A.; Capilato, J.N.; Pitts, C.R.; Joram, J.; Peters, G.N.; Tovar, J.D.; Smajlagic, I.; Siegler, M.A.; Dudding, T.; et al. Carbonyl-Directed Aliphatic Fluorination: A Special Type of Hydrogen Atom Transfer Beats Out Norrish II. *J. Am. Chem. Soc.* **2020**, *142*, 14710–14724. [[CrossRef](#)]
56. Zhu, J.L.; Schull, C.R.; Tam, A.T.; Rentería-Gómez, Á.; Gogoi, A.R.; Gutierrez, O.; Scheidt, K.A. Photoinduced Acylations Via Azolium-Promoted Intermolecular Hydrogen Atom Transfer. *J. Am. Chem. Soc.* **2023**, *145*, 1535–1541. [[CrossRef](#)] [[PubMed](#)]
57. Gruber, H.F. Photoinitiators for Free Radical Polymerization. *Prog. Polym. Sci.* **1992**, *17*, 953–1044. [[CrossRef](#)]
58. Jakubiak, J.; Allonas, X.; Fouassier, J.P.; Sionkowska, A.; Andrzejewska, E.; Linden, L.Å.; Rabek, J.F. Camphorquinone–Amines Photoinitiating Systems for the Initiation of Free Radical Polymerization. *Polymer* **2003**, *44*, 5219–5226. [[CrossRef](#)]
59. Encinas, M.V.; Majmud, C.; Lissi, E.A. Polymerization Photoinitiated by Carbonyl Compounds. IX. Methyl Methacrylate Polymerization Photoinitiated by Anthraquinone in Presence of Triethylamine. *J. Polym. Sci. Part A Polym. Chem.* **1990**, *28*, 2465–2474. [[CrossRef](#)]
60. Kucybała, Z.; Pietrzak, M.; Osmańska, K.; Pączkowski, J. Mechanistic and Kinetic Study of Free Radical Polymerization Photoinitiated by Xanthene Dye-n-Phenylglycine Derivatives Photoredox Pairs. *Pol. J. Chem.* **2005**, *79*, 851–866.
61. Linden, S.M.; Neckers, D.C. Fundamental Properties of Rose Bengal. 25. Bleaching Studies of Rose Bengal Onium Salts. *J. Am. Chem. Soc.* **1988**, *110*, 1257–1260. [[CrossRef](#)]

62. Kabatc, J.; Pietrzak, M.; Paćzkowski, J. Cyanine Borates Revisited. Application of the Marcus Equation for the Description of the Kinetics of Photoinitiated Free Radical Polymerization. IV. *Macromolecules* **1998**, *31*, 4651–4654. [[CrossRef](#)]
63. Bartholomew, R.F.; Davidson, R.S. The Photosensitised Oxidation of Amines. Part I. The Use of Benzophenone as a Sensitiser. *J. Chem. Soc. C* **1971**, *1*, 2342–2346. [[CrossRef](#)]
64. Brimage, D.R.G.; Davidson, R.S.; Steiner, P.R. Use of Heterocyclic Compounds as Photosensitisers for the Decarboxylation of Carboxylic Acids. *J. Chem. Soc. Perkin Trans. C* **1973**, *1*, 526–529. [[CrossRef](#)]
65. Davidson, R.S.; Harrison, K.; Steiner, P.R. The Photosensitised Decarboxylation of Carboxylic Acids by Aromatic Ketones. *J. Chem. Soc. C* **1971**, *1*, 3480–3482. [[CrossRef](#)]
66. Davidson, R.S.; Steiner, P.R. The Photosensitized Decarboxylation of Carboxylic Acids by Benzophenone and Quinones. *J. Chem. Soc. C* **1971**, *1*, 1682–1689. [[CrossRef](#)]
67. Ikeda, S.; Murata, S.; Ishii, K.; Hamaguchi, H. Mechanistic Studies of the Pyrene-Sensitized Photodecomposition of N-Phenylglycine: Acceleration of the Photodecomposition by the Addition of an Electron Acceptor. *Bull. Chem. Soc. Jpn.* **2000**, *73*, 2783–2792. [[CrossRef](#)]
68. Rehm, D.; Weller, A. Kinetics of Fluorescence Quenching by Electron and H-Atom Transfer. *Isr. J. Chem.* **1970**, *8*, 259–271. [[CrossRef](#)]
69. Weller, A. Photoinduced Electron Transfer in Solution: Exciplex and Radical Ion Pair Formation Free Enthalpies and Their Solvent Dependence. *Z. Phys. Chem.* **1982**, *133*, 93–98. [[CrossRef](#)]
70. Marcus, R.A. On the Theory of Electron-Transfer Reactions. VI. Unified Treatment for Homogeneous and Electrode Reactions. *J. Chem. Phys.* **2004**, *43*, 679–701. [[CrossRef](#)]
71. Ebersson, L. *Electron Transfer in Organic Chemistry*; Springer: New York, NY, USA, 1987.
72. Marcus, R.A. Chemical and Electrochemical Electron-Transfer Theory. *Annu. Rev. Phys. Chem.* **1964**, *15*, 155–196. [[CrossRef](#)]
73. Paćzkowski, J.; Pietrzak, M.; Kucybała, Z. Generalization of the Kinetic Scheme for Photoinduced Polymerization via an Intermolecular Electron Transfer Process. 2. Application of the Marcus Theory. *Macromolecules* **1996**, *29*, 5057–5064. [[CrossRef](#)]
74. Sarkis, G.Y.; Al-Badri, H.T. Synthesis and Spectroscopic Studies of Some New Substituted 6H-Indolo[2,3-b]Quinoxalines. *J. Heterocycl. Chem.* **1980**, *17*, 813–815. [[CrossRef](#)]
75. Huynh, T.N.; Tran, D.T.; Nguyen, T.T. Elemental Sulfur Promoted Condensation of Indoles and 1,2-Phenylenediamines. *Tetrahedron Lett.* **2023**, *116*, 154360. [[CrossRef](#)]
76. Manna, K.; Agrawal, Y.K. Microwave Assisted Synthesis of New Indophenazine 1,3,5-Trisubstituted Pyrazoline Derivatives of Benzofuran and Their Antimicrobial Activity. *Bioorganic Med. Chem. Lett.* **2009**, *19*, 2688–2692. [[CrossRef](#)]
77. Avula, S.; Komsani, J.; Koppireddi, S.; Yadla, R.; Kanugula, A.; Kotamraju, S. Synthesis and Cytotoxicity of Novel 6H-Indolo[2,3-b]Quinoxaline Derivatives. *Med. Chem. Res.* **2012**, *22*, 3712–3718. [[CrossRef](#)]
78. Van Dormael, A. Colorants Polyméthaniques Dérivés Du Noyau de La Pyrimidazolone. *Bull. Des. Sociétés Chim. Belg.* **1949**, *58*, 167–182. [[CrossRef](#)]
79. Pyszka, I.; Kucybała, Z. Quinolineimidazopyridinium Derivatives as Visible-Light Photoinitiators of Free Radical Polymerization. *Polymer* **2007**, *48*, 959–965. [[CrossRef](#)]
80. Majhi, B.; Parwez, A.; Palit, S.; Dutta, S. One-Pot Cascade Annulation-Triggered Synthesis of N-6-Substituted Norcryptotackieine Alkaloids and Evaluation of Their Antileishmanial Activities. *J. Org. Chem.* **2022**, *87*, 14695–14705. [[CrossRef](#)] [[PubMed](#)]
81. Rong, G.-Q.; Zhao, J.-Q.; Zhang, X.-M.; Xu, X.-Y.; Yuan, W.-C.; Zhou, M.-Q. One-Pot Access to Indolylchromeno[2,3-b]Indoles via Iodine-Mediated Friedel-Crafts Alkylation/Oxidative Coupling Reaction of Indoles and Salicylaldehydes. *Tetrahedron* **2018**, *74*, 2383–2390. [[CrossRef](#)]
82. Ivashchenko, A.V.; Drushlyak, A.G.; Titov, V.V. Reaction of O-Phenylenediamine with Isatins. *Chem. Heterocycl. Compd.* **1984**, *20*, 537–542. [[CrossRef](#)]
83. Takekuma, S.; Katayama, S.; Takekuma, H. Preparation and Structure of Tetrakis(Indolo[2,3-b]Quinoxalinato)Dinickel(II). *Chem. Lett.* **2000**, *29*, 614–615. [[CrossRef](#)]
84. Kumbhar, A.; Kanase, D.; Mohite, S.; Salunkhe, R.; Lohar, T. Brønsted Acid Hydrotrope Combined Catalysis in Water: A Green Approach for the Synthesis of Indoloquinoxalines and Bis-Tetronic Acids. *Res. Chem. Intermed.* **2021**, *47*, 2263–2278. [[CrossRef](#)]
85. Kanhed, A.M.; Patel, D.V.; Patel, N.R.; Sinha, A.; Thakor, P.S.; Patel, K.B.; Prajapati, N.K.; Patel, K.V.; Yadav, M.R. Indoloquinoxaline Derivatives as Promising Multi-Functional Anti-Alzheimer Agents. *J. Biomol. Struct. Dyn.* **2022**, *40*, 2498–2515. [[CrossRef](#)]
86. Edayadulla, N.; Lee, Y.R. Cerium Oxide Nanoparticle-Catalyzed Three-Component Protocol for the Synthesis of Highly Substituted Novel Quinoxalin-2-Amine Derivatives and 3,4-Dihydroquinoxalin-2-Amines in Water. *RSC Adv.* **2014**, *4*, 11459–11468. [[CrossRef](#)]
87. Pyszka, I.; Skowroński, Ł.; Jędrzejewska, B. Study on New Dental Materials Containing Quinoxaline-Based Photoinitiators in Terms of Exothermicity of the Photopolymerization Process. *Int. J. Mol. Sci.* **2023**, *24*, 2752. [[CrossRef](#)] [[PubMed](#)]

Disclaimer/Publisher's Note: The statements, opinions and data contained in all publications are solely those of the individual author(s) and contributor(s) and not of MDPI and/or the editor(s). MDPI and/or the editor(s) disclaim responsibility for any injury to people or property resulting from any ideas, methods, instructions or products referred to in the content.